crystals

MDPI

Article

Development of Reconfigurable High-Frequency Devices Using Liquid Crystal in Substrate-Integrated Gap Waveguide Technology

Aleksandr Andreyevich Voronov [1], Carmen Bachiller [1,*], Belén Villacampa [2,*] and Vicente E. Boria [1]

[1] Instituto de Telecomunicaciones y Aplicaciones Multimedia, Universitat Politècnica de València, 46022 Valencia, Spain; alvo2@upv.es (A.A.V.); vboria@dcom.upv.es (V.E.B.)
[2] Instituto de Nanociencia y Materiales de Aragón (INMA), CSIC-Universidad de Zaragoza, Departamento de Física de la Materia Condensada, Universidad de Zaragoza, 50009 Zaragoza, Spain
* Correspondence: mabacmar@dcom.upv.es (C.B.); bvillaca@unizar.es (B.V.)

Abstract: This article presents the theoretical study, numerical simulation and fabrication of a phase shifter and a stub resonator for use in microstrip ridge gap waveguide (MRGW) technology, using a liquid crystal (LC) in the substrate as a reconfigurable material. The phase shifter and the stub resonator are filled with LC, and thanks to the LC's dielectric anisotropy properties, the phase shift and the resonance response can be easily controlled using an external electric or magnetic bias field. The phase shifter was designed to operate in the range of 10 to 20 GHz, and the resonator was designed to operate in the range of 7.8 to 8.8 GHz. The phase shifter's responses (including both phase shift and insertion losses), associated with both the parallel and perpendicular permittivity values of the LC, were computed and measured, and then the corresponding figure of merit (FoM) was extracted. The resonator's frequency responses, associated with both the LC's parallel and perpendicular permittivity, were computed. The resonator's frequency responses, which provided different polarization voltages, were measured and compared to the simulation results. All technological issues related to both prototypes are also discussed here. The good agreement between the simulation and measurement results confirm this technology as a viable approach to the practical implementation of these microwave reconfigurable devices.

Keywords: nematic liquid crystal; permittivity; loss tangent; microstrip ridge gap waveguide; high impedance electromagnetic surfaces; microwaves

Citation: Voronov, A.A.; Bachiller, C.; Villacampa, B.; Boria, V.E. Development of Reconfigurable High-Frequency Devices Using Liquid Crystal in Substrate-Integrated Gap Waveguide Technology. *Crystals* **2024**, *14*, 735. https://doi.org/10.3390/cryst14080735

Academic Editor: Benoit Heinrich

Received: 30 July 2024
Revised: 15 August 2024
Accepted: 15 August 2024
Published: 19 August 2024

1. Introduction

Recent advances in new wireless communication platforms (satellite communications, 5G and 6G wireless systems) promise improved coverage, higher capacity and data rates, a more efficient use of spectrum resources and lower latency as well as increased reliability and flexibility [1,2]. The evolution of wireless networks is also driven by the deployment of fiberoptic networks due to an increasing number of subscribers. Future 6G mobile networks are expected to provide improved communication capacities, which would require a substantial increase in terms of bandwidth [3,4].

As higher frequencies are used to transmit information, wireless communications will experience greater propagation losses and blockage effects from obstacles. To address this, electronically steerable antennas will be required, which can be achieved using functional material technologies such as liquid crystals (LCs) [5].

Since high-frequency communications (for present microwave- and millimeter-wave systems and future terahertz applications) necessitate the development of smaller devices, it has been observed that microstrip technology suffers from surface waves and high losses, degrading performance within particularly high frequency spectral ranges. Waveguide technology is also not a cost-effective solution, and poses additional challenges for integration with network hardware (feeding systems and antennas) [6].

Thus, gap waveguide technology has emerged as a potential solution [7], with the ridge gap waveguide being one of the first practical implementations [8]. More recently, several realizations of such technology, also known as the microstrip ridge gap waveguide (MRGW), have been addressed in [9–11]. These technologies offer advantages over the previously mentioned ones, including there being no need for strong mechanical contact between the cover and the body enclosing a waveguide cavity, lower insertion losses, and the suppression of surface standing waves. For these purposes, they make use of an artificial magnetic wall (perfect magnetic conductor, PMC) with a very high surface impedance that provides (together with a top metal lid) an electromagnetic (EM) bandgap where only the fundamental mode (EM fields) can propagate.

In this work, MRGW technology has been chosen because it allows for the integration of functional materials, like the cited LC, with planar technologies based on microstrip lines. Consequently and to attend to the needs of current wireless and satellite communication systems, as well as future 6G networks, a series of compact solutions for MRGW-LC devices have been developed: the phase shifter and the stub resonator.

For a complete analysis, the available EM software tool, CST Studio Suite, v. 2024, will be used. Simulations will be performed using the finite element method to solve the electromagnetic problem of the circuits. Additionally, the eigenvalue solver module will be employed to extract the EM bandgap (with a single-mode propagation region), which can be achieved with the PMC of the considered MRGW.

2. Materials and Methods

This section will present all of the details of the proposed topologies of the considered MRGW-LC microwave circuits. Practical aspects related to the LC material employed, and the coating of an alignment layer on the copper cladding used on commercially printed circuit boards (PCB) are shown. Finally, practical solutions for both reconfigurable components (including assembling and filling steps), as well as the measurement setup, are addressed.

2.1. Fundamentals of Liquid Crystal

Liquid crystals are anisotropic materials that exhibit intermediate phases (mesophases) between solid/crystalline and fluid/isotropic states. In microwave applications, LCs consist of elongated rod-like molecules (calamitic LCs) that typically display a nematic phase at room temperature. In this phase, the molecules flow as liquids but maintain a long-range directional (orientational) order [12].

The use of nematic liquid crystals has the disadvantage that most of them have not been characterized at microwave- and millimeter-wave frequencies (300 MHz–300 GHz), making it difficult to predict their behavior in these high-frequency ranges. However, nematic LCs have not only been used in optical devices but also at microwave frequencies. In the microwave frequency range, where LCs exhibit low losses, they are of great practical interest for implementation in reconfigurable devices. For example, a significant number of scientific articles have reported on steerable antennas [13], phase shifters [14,15] and filters [16,17].

Macroscopically, the anisotropic structure of nematic LCs can be described by a directional vector $\overline{n}$, representing the average direction of the long axis of the LC molecules. The dielectric permittivity of this material is defined by the angle between this director $\overline{n}$ and the applied electric field. Consequently, nematic LCs have two principal permittivity values: parallel to the director $\overline{n}$ ($\varepsilon_{\parallel}$) and perpendicular to the director $\overline{n}$ ($\varepsilon_{\perp}$). The nematic LC mixtures used in this work can exhibit an electric dipole moment, allowing for the reorientation of molecules using a continuous or low-frequency electric field (around 1 kHz), or alternatively a magnetic field. This results in a uniaxial anisotropic material whose permittivity value can be controlled.

At this point, it is necessary to explain how LCs with dielectric anisotropy properties function under the influence of a continuous electric field (1 kHz). An electric field was chosen because it allows for a precise control of its intensity level. The behavior of the LC can be

described based on the corresponding applied voltage. Consider a case with two electrodes coated with an alignment layer, typically made of a material that allows microgrooves to be deposited on its surface. The alignment layer anchors the LC molecules in a specific direction; for instance, in the perpendicular state. Without this, the molecules would be randomly oriented, resulting in an anisotropic LC state with no discernible pattern.

As shown in Figure 1, which presents a cross section of the phase shifter device described in Ssection 2.5, the LC molecules begin to rotate when the bias voltage (V_b) applied between the two electrodes exceeds the Fréedericks threshold value (V_{th}) [12]. When the director $\overline{n}$ of the LC molecules forms a perpendicular angle to the polarization field ($\overline{E}_{RF}$), the permittivity of the perpendicular state ($\varepsilon_\perp$) is achieved ($V_b < V_{th}$), as shown in Figure 1a. The threshold voltage V_{th} depends on the elastic constant of extension K_{11} and the electrical anisotropy $\Delta\epsilon_{r,1kHz}$, as shown in Equation (1). As V_b increases, it reaches the saturation state ($V_b = V_{\text{sat}}$), thus resulting in the LC molecules being fully aligned to the parallel state and achieving the parallel permittivity $\epsilon_\parallel$, see Figure 1b. On the other hand, when the bias voltage exceeds the Fréedericks threshold ($V_b > V_{th}$), intermediate permittivity values between the two extreme states $\varepsilon_\perp$ and $\varepsilon_\parallel$ can be achieved.

$$V_{th} = \pi \sqrt{\frac{K_{11}}{\epsilon_0 * \Delta\epsilon_{r,1kHz}}}, \tag{1}$$

In this work, nematic LC mixtures, from the company Merck, Darmstadt, Germany, will be used, specifically the models "GT3-23002" and "GT7-29001". The LC EM properties provided by the manufacturer (measured at 19 GHz) are the dielectric constant and loss tangent (whose values are collected, for both polarization states, in Table 1). Last but not least, it is necessary to highlight that the PMC used (together with the top metal lid) to confine the EM field by the LC substrate is framed in red in Figure 1. The topology and design of this PMC is detailed next.

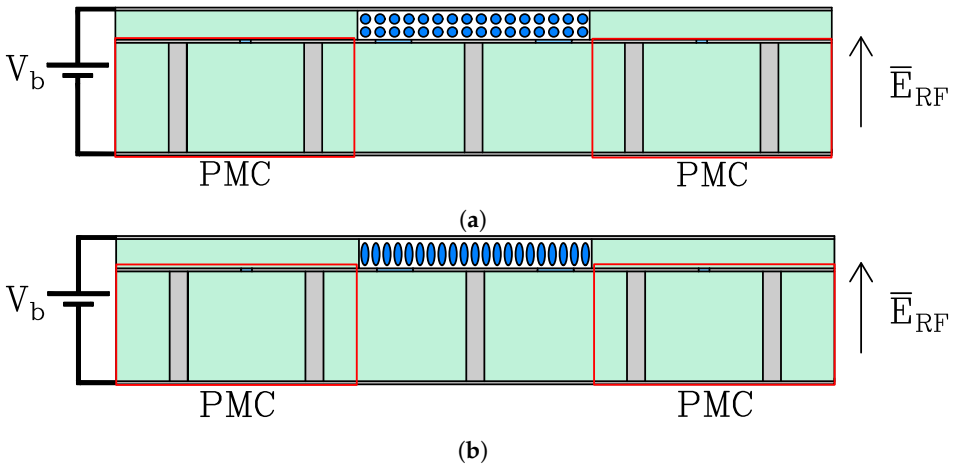

Figure 1. Polarization of the LC in the nematic state: (**a**) $V_b < V_{th}$, (**b**) $V_b \geq V_{sat}$.

Table 1. EM properties of commercial LC mixtures measured at 19 GHz.

	GT3-23002	**GT7-29001**
$\epsilon_\parallel$	3.02	3.53
$\epsilon_\perp$	2.36	2.45
$\tan(\delta_\parallel)$	0.0035	0.0064
$\tan(\delta_\perp)$	0.0128	0.00117

2.2. Design of the High Impedance Surface (HIS)

The dispersion diagram of a metasurface (or periodic structure) shown below shows the frequency regions where the related Floquet–Bloch modes can not propagate (the so

called EM bandgaps) [18]; in particular, and in the context of this work, the HIS provides the condition of a PMC [19], and is recreated in practice by an array of metallized "mushroom" cells as can be seen in Figure 2a.

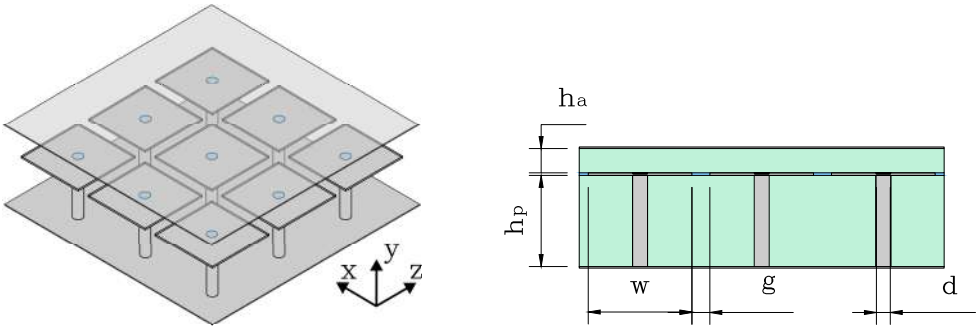

(**a**) (**b**)

Figure 2. Topology of the high impedance surface: (**a**) an array of "mushroom" cells, (**b**) transversal cut of an array of "mushroom" cells.

2.2.1. Parametric Analysis

To conduct the parametric analysis of the HIS unit cell, CST Studio Suite v. 2024 was used. The dispersion diagram illustrates the propagation constant on the two dimensional axes (Ox, Oz) of the periodically extended "mushroom" base cell, Figure 2a. The cited dispersion diagram is obtained with the CST Studio Suite eigenmode solver module, which computes the EM field eigenmodes at specific frequencies without external excitation. The dispersion curves were plotted along a specified path, representing EM wave solutions with different components in the Ox and Oz directions. Next, we will detail the parameters influencing the variation in the frequency range of the EM bandgap.

According to [20], the parameters controlling the response (EM bandgap) of an array of metallic "mushrooms" are as follows (see their geometrical meaning in Figure 2b:

- The diameter of the via (d) is directly proportional to the minimum frequency of the upper mode and to the maximum frequency of the lower mode. Consequently, when (d) is increased, the resonance frequency of the PMC is increased as well. Moreover, since the minimum frequency of the upper mode increases more than that of the maximum frequency of the lower mode, a wider bandwidth is achieved.
- The height of the lower substrate (h_p) inversely affects the maximum frequency of the lower mode. Therefore, increasing the height of the lower substrate increases the bandwidth.
- The height of the upper substrate (h_a) directly affects the maximum frequency of the lower mode. Thus, increasing the height of the upper substrate reduces the bandwidth of the EM bandgap.
- Material permittivity (ϵ_r) directly affects the maximum frequency of the lower mode, thereby reducing the bandwidth of the EM bandgap.
- Patch dimensions (w) inversely affect both the maximum frequency in the lower mode and the minimum frequency in the upper mode of the EM bandgap. Moreover, since the minimum frequency in the upper mode increases more than the maximum frequency in the lower mode, the bandwidth of the EM bandgap widens.

The frequency range considered for the reconfiguration of the bandpass responses of both MRGW-LC devices was from 7 GHz to 20 GHz. The two substrates used were RO4003C with a permittivity of 3.55, where the height of the lower substrate is $h_p = 1.524$ mm (corresponds to bottom PCB) and the one of the upper substrate is $h_a = 0.406$ mm (corresponds to top PCB).

A parametric experiment was conducted using, as indicated above, the eigenmode solver module of the CST Studio Suite v. 2024. The periodic structure was studied by

varying the field vectors k_x and k_z along Ox and Oz directions. Dispersion curves along with the EM bandgap were calculated, as illustrated in Figure 3.

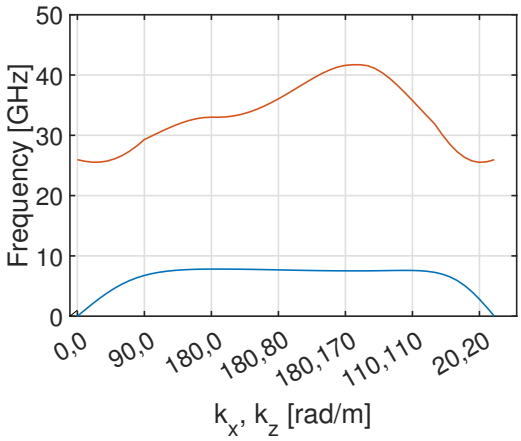

Figure 3. The scatter plot of HIS.

After successive iterations, an EM bandgap between 7 GHz and 25 GHz was achieved. The final solution for the considered HIS design parameters is presented in Table 2.

Table 2. HIS's design parameters.

Parameter	Value [mm]
h_a	0.406
h_p	1.524
g	0.300
w	1.734
d	0.250

2.3. Proposed Coupling Network

The complete design includes a matching network between the coaxial cable and the device under test (DUT). The "1092-01A-6 Southwest" connector has been chosen to match the coaxial cable to the input microstrip line. Additionally, the matching network includes an exponential taper to match the 50 Ω microstrip line input impedance to the 35 Ω MRGW-LC circuit impedance (of the phase shifter or the stub resonator), as can be seen in Figure 4, where the widths (w_{ms} and w_{lin}) are those corresponding to the two cited planar lines. The design parameters of the MRGW-LC coupling network are presented in Table 3.

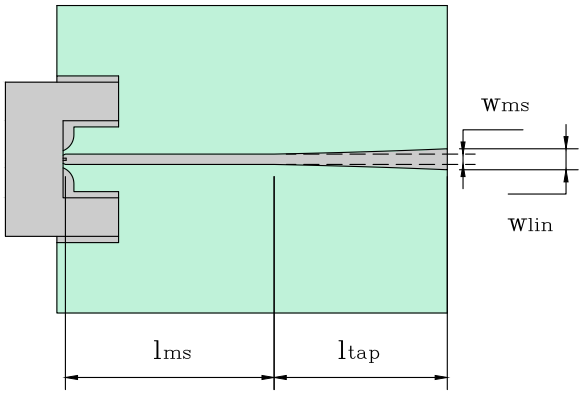

Figure 4. MRGW-LC coupling network.

Table 3. MRGW-LC coupling network's design parameters.

Parameter	Value [mm]
w_{ms}	0.850
w_{lin}	1.728
l_{ms}	14.000
l_{tap}	14.266

Impedance Approximation Using a Stripline Equivalence

To theoretically determine the characteristic impedance of the MRGW-LC line, we have used the model proposed in [21], where an equivalent stripline solution is considered. Thus, the width of the MRGW line is directly related to the width of the equivalent stripline model.

An equivalence can be established between the MRGW line and the stripline, see Equation (2).

$$Z_{0,MRGW} \approx 2 * Z_{0,Strip} \tag{2}$$

And, therefore, it can be assumed that, for the corresponding line widths, the following Equation (3) holds true.

$$w_{lin} \approx 2 * w_{strip} \tag{3}$$

The width of the stripline given the characteristic impedance remains to be calculated. It can be determined as shown in Equation (4).

$$\frac{w_{strip}}{b} = \begin{cases} x & \text{for} \sqrt{\epsilon_r} Z_0 < 120\,\Omega \\ 0.85 - \sqrt{0.6 - x} & \text{for} \sqrt{\epsilon_r} Z_0 > 120\,\Omega \end{cases} \tag{4}$$

2.4. Calibration Kit Design

In order to exclude the effects of the feeding network, including the microstrip section (regarding insertion losses, phase, etc.) when measuring S-parameters with a Vector Network Analyzer (VNA), a Thru–Reflect–Line (TRL) calibration kit has been designed considering the following aspects [22]:

1. Reflect (open): the length of the microstrip section is used, leaving approximately 10 mm spacing between open sections.
2. Thru: twice the length of the microstrip line is used.
3. Line: an electrical length of approximately 90º is employed (considering top PCB's upper substrate, with the height of $h_a = 0.406$ mm, at 11 GHz, see Section 2.2.1).

Additionally, for the initial measurements and to validate the manufactured TRL calibration kit, a TOSM (Thru–Open–Short–Match) calibration kit with reference "Agilent 85052D" was used. Figure 5 presents the top view of the TRL kit with the involved dimensional parameters, and Table 4 summarizes their optimal values after the final design.

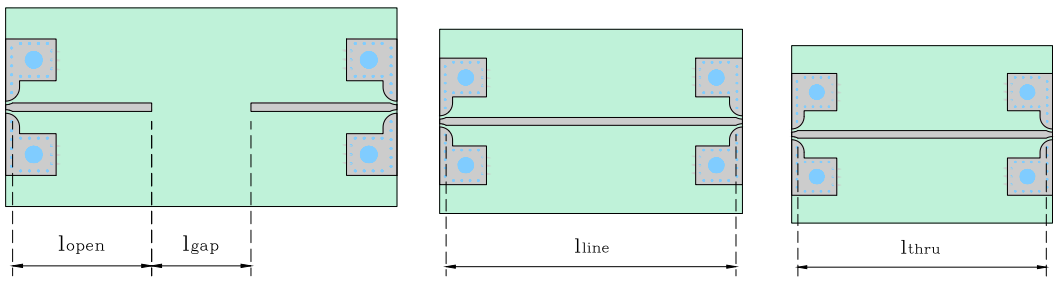

(**a**) (**b**) (**c**)

Figure 5. TRL calibration kit: (**a**) open, (**b**) line, (**c**) thru.

Table 4. TRL calibration kit design parameters.

Parameter	Value [mm]
l_{line}	31.473
l_{thru}	28.000
l_{open}	14.000
l_{gap}	10.000

2.5. MRGW-LC Phase Shifter

The design was implemented using three PCBs, see Figure 1, where the bottom PCB contains the periodic "mushroom" cell structure and the MRGW-LC line, the top PCB contains the LC's bathtub and the third PCB covers the top PCB with the metal lid, or more specifically, with the copper cladding (the third PCB consists of the same substrate with height of h_p, see Section 2.2.1, to give the structure mechanical rigidity), which also contains the filler holes for the LC. The LC's bathtub is formed by internally cutting the upper substrate. Then, the bottom PCB is joined (using screws) with the top PCB containing the LC's bathtub and with metal lid. A simulation of a section of the MRGW-LC phase shifter line has been carried out using the CST Studio Suite v. 2024 solver, to extract the effective wavelength at 11 GHz and therefore to estimate the value of l_{cl}, the length of the LC's bathtub, which we chose to be approximately two wavelengths at this frequency, $l_{cl} = 24.467$ mm. This value was chosen to provide a clearer comparison between the filled and unfilled MRGW-LC devices. The topology of the proposed phase shifter is given in Figure 6.

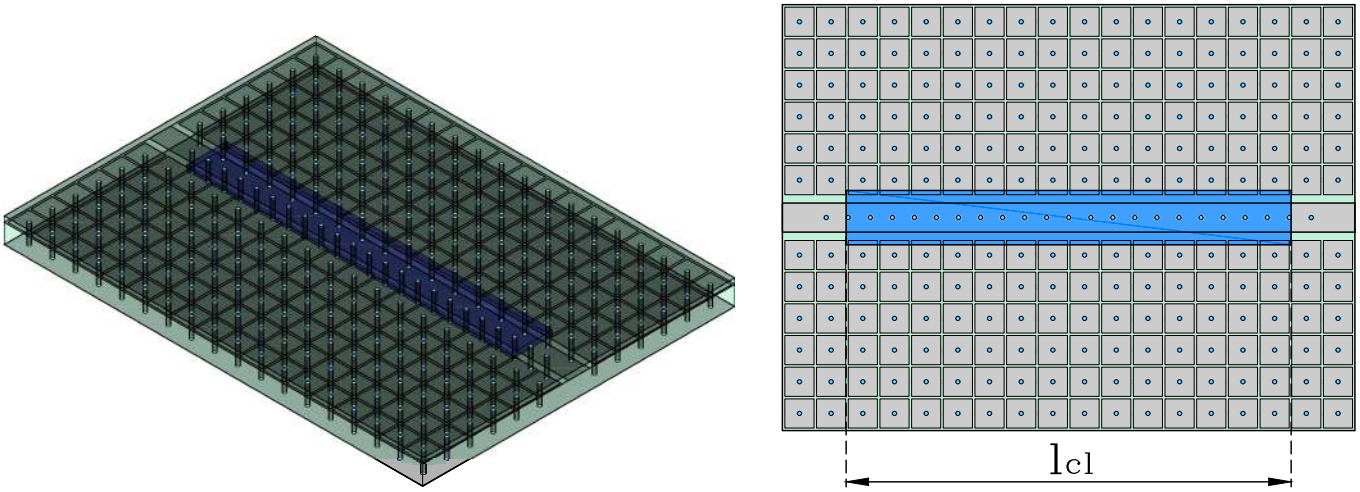

(**a**) (**b**)

Figure 6. MRGW-LC phase shifter: (**a**) isometric view; (**b**) top view.

2.6. MRGW-LC Stub Resonator

The MRGW-LC resonator was implemented using stub configuration (coupled in parallel to the main MRGW-LC feeding line). Since the resonator extends half the wavelength [23], and by evaluating a section of the MRGW-LC phase shifter line in CST Studio Suite v. 2024 (the same procedure as in Section 2.5), the effective wavelength was deduced and thus the resonator's length was determined. Finally, the model was evaluated and the results are presented in Table 5; the topology is given in Figure 7.

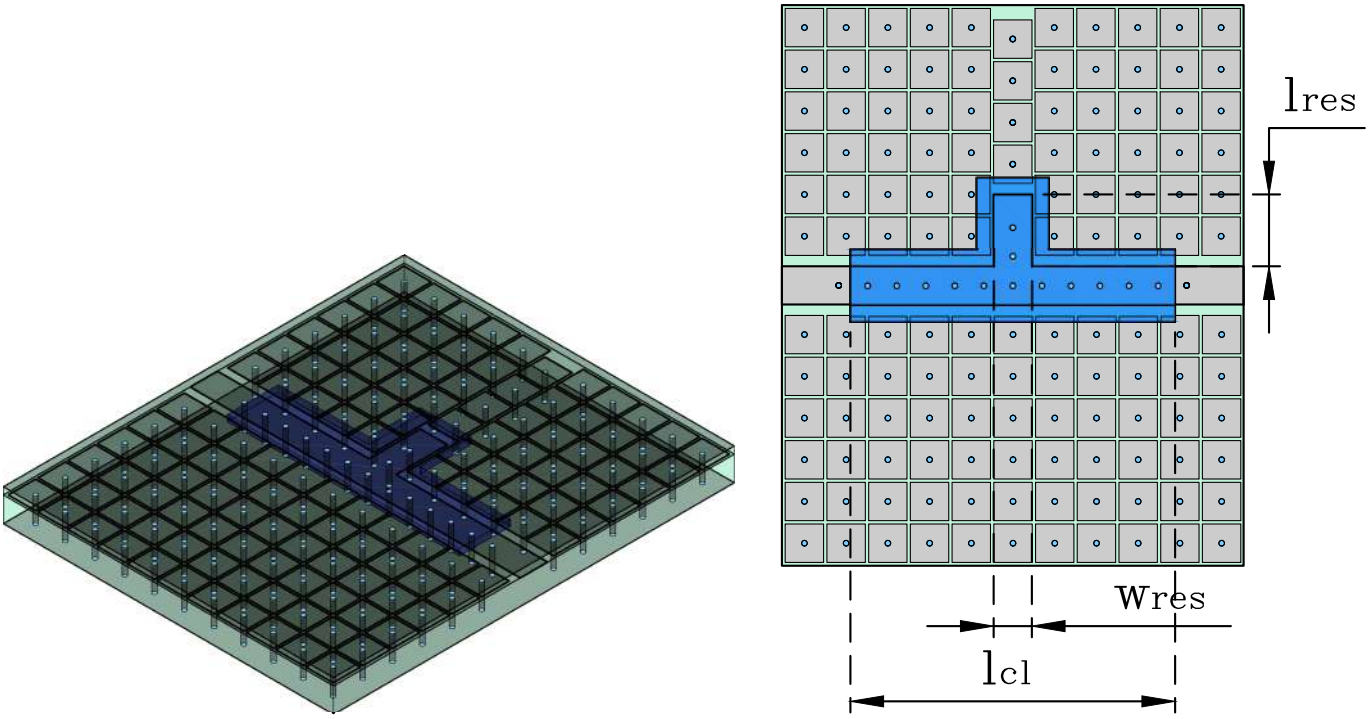

(**a**) (**b**)

Figure 7. MRGW-LC stub resonator: (**a**) isometric view; (**b**) top view.

Table 5. MRGW-LC stub resonator's design parameters.

Parameter	Value [mm]
l_{res}	3.247
w_{res}	1.728
l_{cl}	14.669

2.7. Alignment Layer

The alignment layer coating is typically formed by depositing polyimide (PI), a polymeric resin composed of repetitive imide units, on the liquid crystal support, usually glass, followed by creating microgrooves through rubbing in a defined direction. However, when applying this layer on a rougher substrate such as copper, the significant surface roughness can obscure the microgrooves of the alignment layer, potentially causing malfunction. In such cases, a thicker layer of PI is commonly used [24,25].

Polyimide Deposition

The PI was applied onto the circuit using a pipette and distributed via spin coating. Prior to this, a Kapton mask was used to prevent PI deposition on the "mushroom" bed. This procedure produced a uniform layer of approximately 500 nm thick. The initial curing was performed at 80 °C for 20 min, followed by a second curing at 180 °C for 1 h; next, Kapton mask was removed by carefully cutting around the edges of the masking tape. As a result, the samples were covered and allowed to rest for a couple of hours, and subsequently, velvet rubbing was performed to create microgrooves on the alignment layer. Finally, to ensure that the rubbing process created microgrooves, a microscope was used to perform the measurements. It was confirmed that fine microgrooves had been created on the alignment layer, as observed in Figure 8 (which represents a fragment of the MRGW-LC resonator).

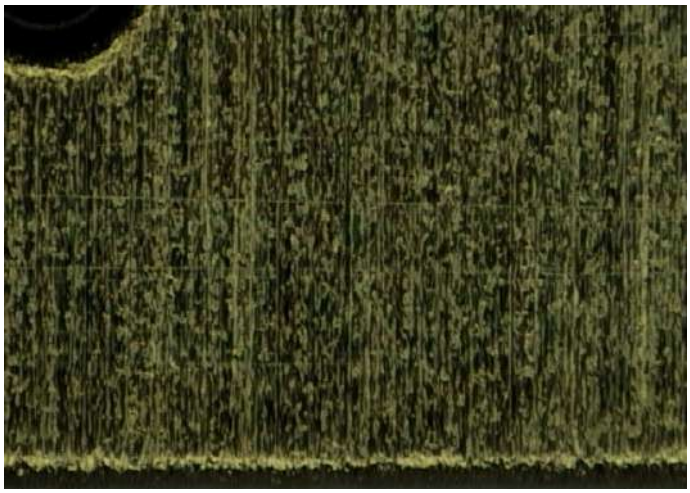

Figure 8. MRGW-LC resonator's microscope image with microgrooves.

2.8. Assembling and Filling

The three PCBs of the MRGW-LC devices were assembled by welding and screwing. A low-temperature, no-clean solder paste (SMDLTLFP10T5 from Chipquik) was used to assemble the stack. Then, "1092-01A-6 Southwest" 2.92 mm female coax connectors for the RF signal were screwed to the ports, and Bias Tee (SHF BT45-R) was used to couple the DC electrical signal to the RF electrical signal. The frequency response (transmission S_{21} and reflection S_{11} parameters) of the empty MRGW-LC devices were measured to verify the device's functionality; the results can be seen in Section 3. The MRGW-LC's devices were then filled with GT3-23002 and GT7-29001 liquid crystals using a syringe and sealed on the exterior of the structure with NOA-61 optical glue. The assembled devices and the TRL calibration kit are presented in Figure 9.

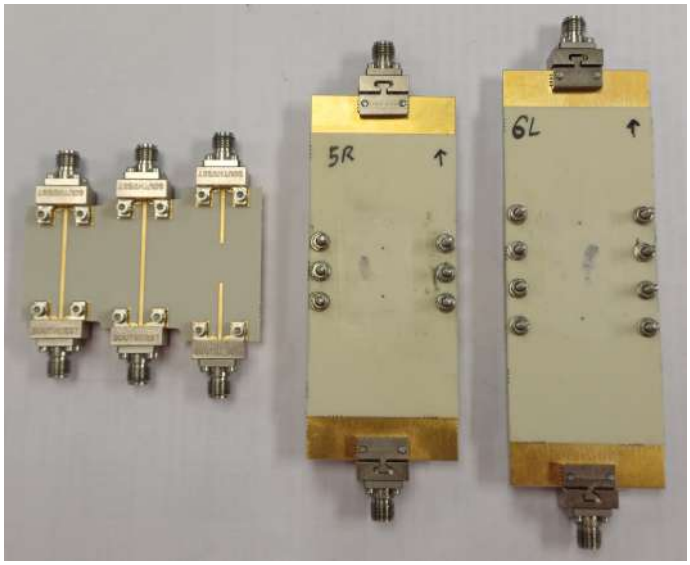

Figure 9. MRGW-LC devices (from left to right): TRL calibration kit, stub resonator, phase shifter.

2.9. Measurement Setup

The experimental setup required a low-frequency signal generator and an AC voltage amplifier to generate the required bias signal (a sinusoidal wave of 1 kHz), which was varied from 0 to 125 V_{pp}, during the measurement. Here, 0 Vpp, i.e., no bias voltage applied, corresponds to the perpendicular state of LC molecules (see Figure 1a from Section 2.1) and 125 Vpp, i.e., bias voltage reaching the saturation state, $V_b > V_{sat}$, corresponds to the parallel state of the LC molecules (see Figure 1b from Section 2.1).

The amplified low-frequency signal was then fed to the bias tee, which combined it with the RF signal from a VNA. The frequency response of the resonator was measured at different bias voltages using a VNA with additional DC blocks to protect the equipment. Figure 10 shows the whole measurement setup.

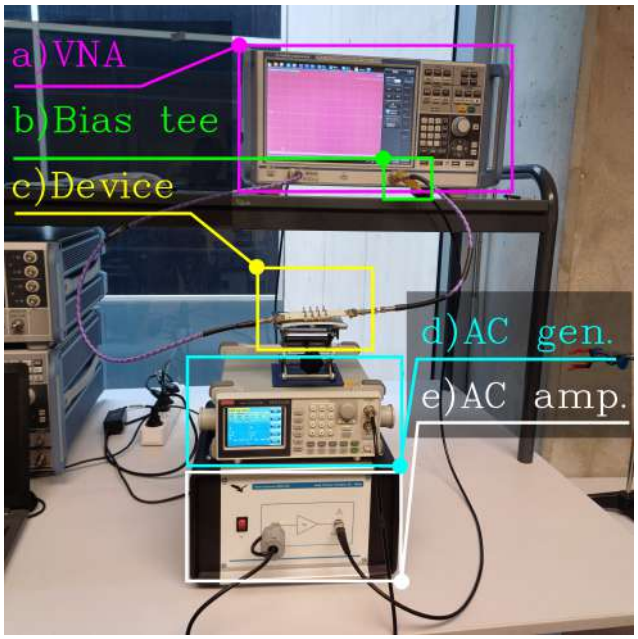

Figure 10. Measurement setup: (**a**) VNA, (**b**) bias tee, (**c**) device under test, (**d**) AC signal generator, (**e**) AC voltage amplifier.

3. Results and Discussion

The electrical responses of the MRGW-LC devices considered in this study lack a theoretical (analytical) solution due to their complex geometries and the multiple dielectric materials (RO4003 substrate and LC) involved. Therefore, the structure was simulated (numerically) using the commercial software CST Studio Suite v. 2024, using the electrical properties of the LC given by the provider Merck, Darmstadt, Germany.

Firstly, in order to ensure that the manufactured devices agree with the simulation results, measurements were made in a vacuum conditions, i.e., without filling the devices with LC, as shown in Figure 11. It is necessary to note at this point that the frequency response of the phase shifter device has a good agreement with the simulated response. However, the resonator device's response, in comparison to the simulated one, shifted from $f_{0,sim} = 11$ GHz towards $f_{0,meas} = 11.5$ GHz due to manufacturing tolerances.

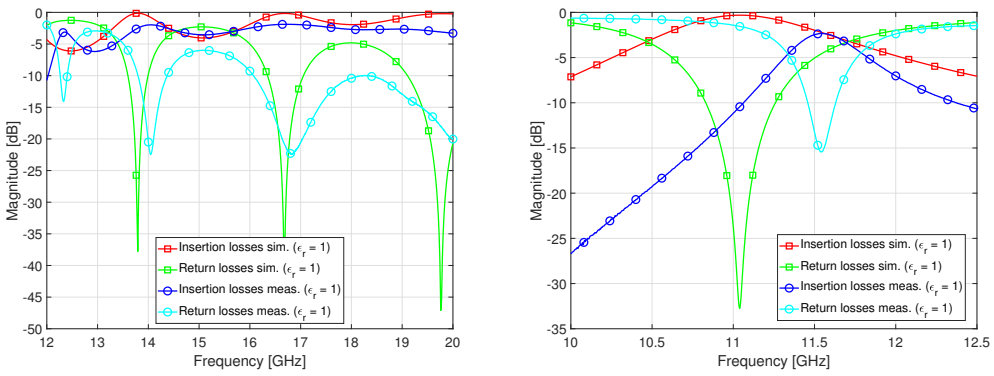

Figure 11. MRGW-LC devices' frequency response measured in vacuum conditions: (**a**) phase shifter; (**b**) stub resonator.

Secondly, the devices were filled with GT3-23002 and GT7-29001 and the measurements were performed. The numerical results obtained through simulations were compared with the measured data and then some conclusions were drawn. As can be seen from the Figure 12, the measured reconfigurability range of GT3-23002 is 4.08% (f_{0Vpp}= 9.25 GHz and $f_{V_{max}}$ = 8.88 GHz) and that of GT7-29001 is 4.82% (f_{0Vpp} = 10.20 GHz and $f_{V_{max}}$ = 9.72 GHz). In contrast, the simulated reconfigurability range of GT3-23002 is 7.60% (f_{0Vpp} = 8.74 GHz and $f_{V_{max}}$ = 8.10 GHz) and that of GT7-29001 is 10.72% (f_{0Vpp} = 8.65 GHz and $f_{V_{max}}$ = 7.77 GHz). It is noticeable from these results that the resonator is not completely filled, as can be seen from the small range of resonant frequencies for the measured results in comparison with the one for the simulated data.

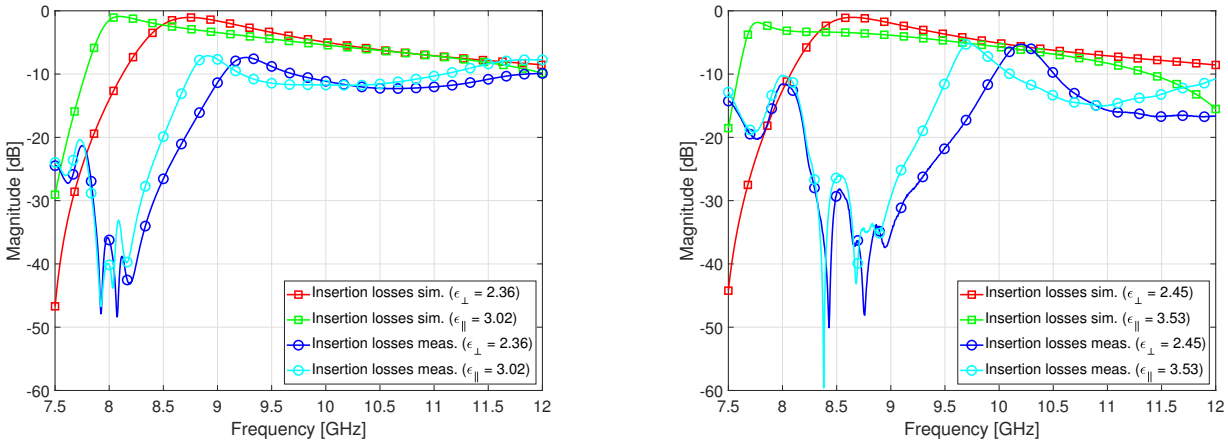

(**a**) (**b**)

Figure 12. Comparison of the frequency responses of the simulated and measured responses of the resonator filled with (**a**) GT3-23002 and (**b**) GT7-29001.

For the phase shifter devices, Figure 13 clearly shows that the phase shift results of the GT3-23002 fit well with the simulation, following a periodic pattern with the mean of approximately 70° of phase shift. Similarly, the measured phase pattern of the GT7-29001, exhibits a linear trend similar to the simulated one, but with a slight decrease in phase shift compared to the results of numerical simulation, with a mean of approximately 75° of phase shift. The GT3-23002- and GT7-29001-filled devices exhibited significant values for the insertion losses compared to the simulated ones, see Figure 14, although it should be noticed that the measured losses are lower for the GT7-29001 phase shifter.

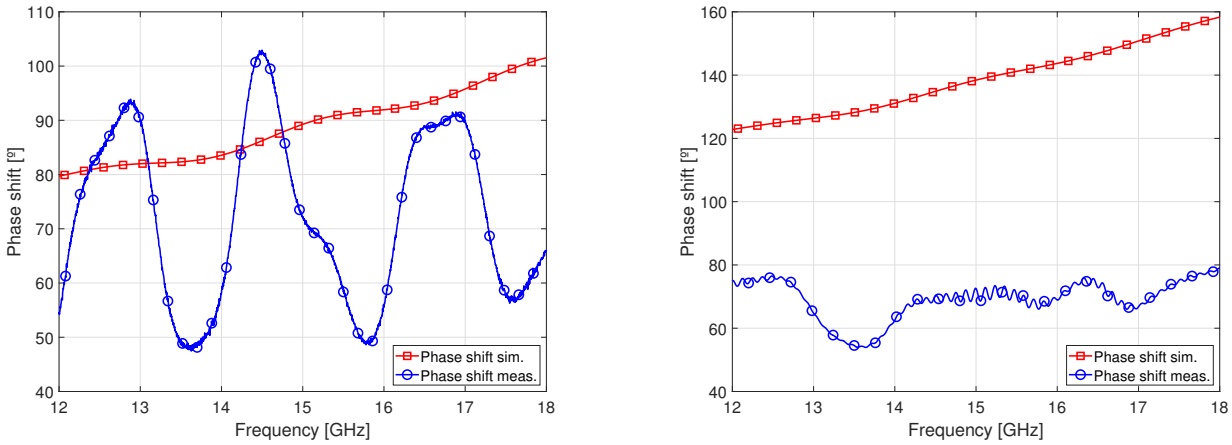

(**a**) (**b**)

Figure 13. Phase shift comparison between the simulated and measured responses of the phase shifter filled with (**a**) GT3-23002 and (**b**) GT7-29001.

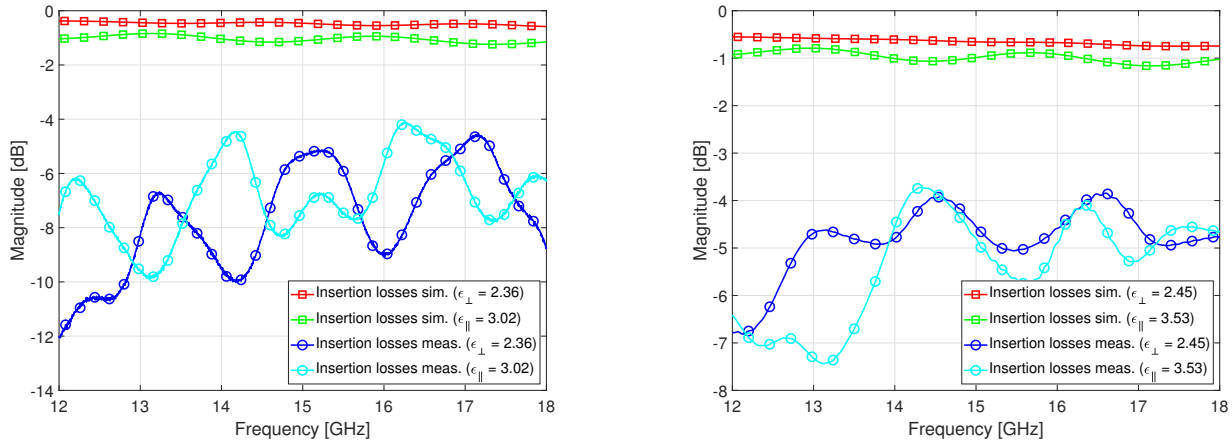

(**a**) (**b**)

Figure 14. Insertion losses comparison between the simulated and measured responses of the phase shifter filled with (**a**) GT3-23002 and (**b**) GT7-29001.

We define figure of merit (FoM) as the maximum ratio of the phase shift and the insertion losses. Thus, both perpendicular-state and parallel-state FoM can be computed and measured, Figure 15. It can clearly be seen that, due to high insertion losses, the phase shifter measured with GT3-23002 presents a mean of 10° per every 1 dB of losses in both the perpendicular and parallel states and the one measured with GT7-29001 a mean of 14° per every 1 dB of losses (in both the perpendicular and parallel states).

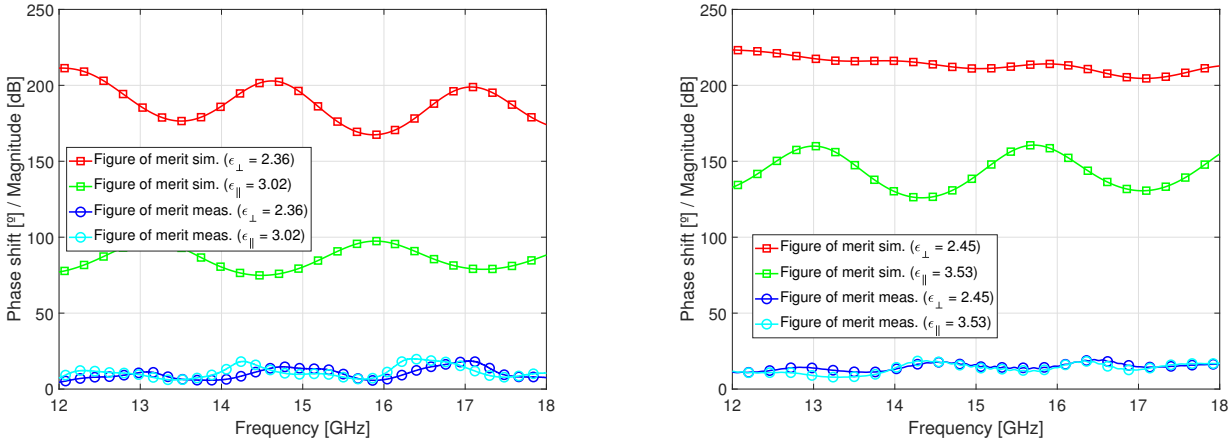

(**a**) (**b**)

Figure 15. Figure of merit comparison between the simulated and measured responses of the phase shifter filled with (**a**) GT3-23002 and (**b**) GT7-29001.

4. Conclusions

The aim of this work was to develop miniaturized microwave devices using a new substrate-integrated gap waveguide technology, that allows the suppression of travelling waves and the use of functional materials for implementing frequency reconfigurability. The proposed phase shifter and resonator devices are developed and manufactured by layers, conforming in one of them the cavities to be filled with two commercial LC mixtures (GT3-23002 and GT7-29001 form Merck, Darmstadt, Germany). For the accurate operability of the MRGW-LC devices, they were sealed with NOA-61 optical glue (to avoid accidental LC leakage) and the alignment layers were properly coated.

The devices were then fed by an RF signal coupled with the variable bias voltage to measure their reconfigurable electrical responses. In general, positive results have been obtained in all cases. Although the measurements of frequency response, phase shift

and FoM of two of the LC mixtures were achieved, there are challenges that have been discovered, particularly related to waterproofing the device to avoid any potential LC leakages. This problem should be addressed in order to guarantee that the DUT remains filled and waterproof so as to obtain better quality results. Thus, the development of compact devices based on MRGW-LC will allow for the integration of microwave devices with LC if this implementation challenge is overcome.

Author Contributions: Conceptualization, C.B. and A.A.V.; methodology, C.B.; software, A.A.V.; validation, C.B., V.E.B. and A.A.V.; formal analysis, C.B. and A.A.V.; investigation, C.B., B.V. and A.A.V.; resources, B.V.; data curation, A.A.V.; writing—original draft preparation, A.A.V.; writing—review and editing, A.A.V., C.B. and V.E.B.; visualization, A.A.V.; supervision, C.B.; project administration, A.A.V. and C.B.; funding acquisition, V.E.B. All authors have read and agreed to the published version of the manuscript.

Funding: This research received no external funding.

Data Availability Statement: The original contributions presented in the study are included in the article, further inquiries can be directed to the corresponding authors.

Acknowledgments: This work has been supported by Ministerio de Ciencia, Innovación y Universidades (Spanish Government) through the R&D Projects PID2022-136590OB-C41 (under grant AEI/10.13039/501100011033/FEDER, UE) and TED2021-129196B-C41 (under grant 10.13039/501100011033/Unión Europea NextGenerationEU/PRTR). The authors thank the financial support from Gobierno de Aragón-Fondo Social Europeo (E47-23R) and from Universidad de Zaragoza (UZ2023-CIE-01).

Conflicts of Interest: The authors declare no conflicts of interest.

Abbreviations

The following abbreviations are used in this manuscript:

AC	Alternate Current
DC	Direct Current
DUT	Device Under Test
EM	Electromagnetic
FoM	Figure of Merit
HIS	High Impedance Surface
LC	Liquid Crystal
MEMS	Microelectromechanical Systems
MRGW	Microstrip Ridge Gap Waveguide
MRGW-LC	Microstrip Ridge Gap Waveguide with Liquid Crystal
PCB	Printed Board Circuits
PI	Polyimide
PMC	Perfect Magnetic Conductor
RF	Radio Frequency
TOSM	Thru–Open–Short–Match
TRL	Thru–Reflect–Line
VNA	Vectorial Network Analyzer

References

1. Monserrat, J.F.; Martin-Sacristan, D.; Bouchmal, F.; Carrasco, O.; Flores de Valgas, J.; Cardona, N. Key Technologies for the Advent of the 6G. In Proceedings of the 2020 IEEE Wireless Communications and Networking Conference Workshops (WCNCW), Seoul, Republic of Korea, 25–28 May 2020; pp. 1–6.
2. Xiao, M.; Mumtaz, S.; Huang, Y.; Dai, L.; Li, Y.; Matthaiou, M.; Karagiannidis, G.K.; Björnson, E.; Yang, K.; Chih-Lin, I.; et al. Millimeter Wave Communications for Future Mobile Networks. *IEEE J. Sel. Areas Commun.* **2017**, *35*, 1909–1935. [CrossRef]
3. Osseiran, A.; Monserrat, J.F.; Marsch, P. (Eds.) *5G Mobile and Wireless Communications Technology*; Cambridge University Press: Cambridge, UK, 2016.
4. Tataria, H.; Shafi, M.; Molisch, A.F.; Dohler, M.; Sjöland, H.; Tufvesson, F. 6G Wireless Systems: Vision, Requirements, Challenges, Insights, and Opportunities. *arXiv* **2021**, arXiv:2008.03213.
5. Ferrari, P. *Reconfigurable Circuits and Technologies for Smart Millimeter-Wave Systems*; EuMA High Frequency Technologies Series; Cambridge University Press: Cambridge, UK, 2022.

6. Herrick, K.; Yook, J.; Katehi, L. Microtechnology in the development of three-dimensional circuits. *IEEE Trans. Microw. Theory Tech.* **1998**, *46*, 1832–1844. [CrossRef]
7. Kildal, P.S.; Alfonso, E.; Valero-Nogueira, A.; Rajo-Iglesias, E. Local Metamaterial-Based Waveguides in Gaps Between Parallel Metal Plates. *IEEE Antennas Wirel. Propag. Lett.* **2009**, *8*, 84–87. [CrossRef]
8. Kildal, P.S.; Zaman, A.; Rajo-Iglesias, E.; Alfonso, E.; Valero-Nogueira, A. Design and experimental verification of ridge gap waveguide in bed of nails for parallel-plate mode suppression. *IET Microw. Antennas Propag.* **2011**, *5*, 262–270. [CrossRef]
9. Birgermajer, S.; Janković, N.; Radonić, V.; Crnojević-Bengin, V.; Bozzi, M. Microstrip-Ridge Gap Waveguide Filter Based on Cavity Resonators With Mushroom Inclusions. *IEEE Trans. Microw. Theory Tech.* **2018**, *66*, 136–146. [CrossRef]
10. Hassan, A.T.; Moharram, M.A.; Kishk, A.A. Empirical Analysis Formulae of Microstrip Ridge Gap Waveguide. In Proceedings of the 2018 IEEE International Symposium on Antennas and Propagation and USNC/URSI National Radio Science Meeting, Boston, MA, USA, 8–13 July 2018; pp. 423–424.
11. Hassan, A.T.; Moharram Hassan, M.A.; Kishk, A.A. Modeling and Design Empirical Formulas of Microstrip Ridge Gap Waveguide. *IEEE Access* **2018**, *6*, 51002–51010. [CrossRef]
12. Wu, S.; Yang, D.K. *Fundamentals of Liquid Crystal Devices*; John Wiley & Sons: Hoboken, NJ, USA, 2006.
13. Reese, R.; Polat, E.; Tesmer, H.; Strobl, J.; Schuster, C.; Nickel, M.; Granja, A.B.; Jakoby, R.; Maune, H. Liquid Crystal Based Dielectric Waveguide Phase Shifters for Phased Arrays at W-Band. *IEEE Access* **2019**, *7*, 127032–127041. [CrossRef]
14. Muller, S.; Scheele, P.; Weil, C.; Wittek, M.; Hock, C.; Jakoby, R. Tunable passive phase shifter for microwave applications using highly anisotropic liquid crystals. In Proceedings of the 2004 IEEE MTT-S International Microwave Symposium Digest (IEEE Cat. No.04CH37535), Fort Worth, TX, USA, 6–11 June 2004; Volume 2, pp. 1153–1156.
15. Weil, C.; Luessem, G.; Jakoby, R. Tunable inverted-microstrip phase shifter device using nematic liquid crystals. In Proceedings of the 2002 IEEE MTT-S International Microwave Symposium Digest (Cat. No.02CH37278), Seattle, WA, USA, 2–7 June 2002; Volume 1, pp. 367–371.
16. Liu, Y.; Jiang, D.; Li, X.; Wang, Z.; Ran, P.; Fu, Z. Microwave CSIW Filter Based on The High Anisotropy Electro-Optic Nematic Liquid Crystal. In Proceedings of the 2019 International Conference on Microwave and Millimeter Wave Technology (ICMMT), Guangzhou, China, 19–22 May 2019; pp. 1–3.
17. Polat, E.; Reese, R.; Jost, M.; Schuster, C.; Nickel, M.; Jakoby, R.; Maune, H. Tunable Liquid Crystal Filter in Nonradiative Dielectric Waveguide Technology at 60 GHz. *IEEE Microw. Wirel. Components Lett.* **2019**, *29*, 44–46. [CrossRef]
18. Brillouin, L. *Wave Propagation in Periodic Structures Electric Filters and Crystal Lattices*; McGraw-Hill: New York, NY, USA, 1946.
19. Sievenpiper, D.; Zhang, L.; Broas, R.; Alexopolous, N.; Yablonovitch, E. High-impedance electromagnetic surfaces with a forbidden frequency band. *IEEE Trans. Microw. Theory Tech.* **1999**, *47*, 2059–2074. [CrossRef]
20. Palomar Cosín, E. Diseño e Implementación de una Línea Gap Ridge Waveguide Integrada en Sustrato con Cristal Líquido. Ph.D. Thesis, Valencia Polytechnic University, Valencia, Spain, 2021.
21. Alfonso, E.; Kildal, P.S.; Valero-Nogueira, A.; Baquero, M. Study of the characteristic impedance of a ridge gap waveguide. In Proceedings of the 2009 IEEE Antennas and Propagation Society International Symposium, North Charleston, SC, USA, 1–5 June 2009; pp. 1–4.
22. Hiebel, M. *Vector Network Analyzer (VNA) Calibration: The Basics*; Rohde & Schwarz: Columbia, MD, USA, 2008.
23. Pozar, D. *Microwave Engineering*; Wiley: Hoboken, NJ, USA, 2012.
24. Zografopoulos, D.C.; Ferraro, A.; Beccherelli, R. Liquid-Crystal High-Frequency Microwave Technology: Materials and Characterization. *Adv. Mater. Technol.* **2019**, *4*, 1800447. [CrossRef]
25. Yazdanpanahi, M.; Bulja, S.; Mirshekar-Syahkal, D.; James, R.; Day, S.E.; Fernandez, F.A. Measurement of Dielectric Constants of Nematic Liquid Crystals at mm-Wave Frequencies Using Patch Resonator. *IEEE Trans. Instrum. Meas.* **2010**, *59*, 3079–3085. [CrossRef]